S,O-functionalized metal-organic frameworks as heterogeneous single-site catalysts for the oxidative alkenylation of arenes via C- H activation

S,O-Functionalized Metal-Organic Frameworks as Heterogeneous Single-Site Catalysts for the Oxidative Alkenylation of Arenes via C-H activation

Niels Van Velthoven,[a] Mickaël Henrion,[a] Jesse Dallenes,[a] Andraž Krajnc,[b] Aram L. Bugaev,[c,d] Pei Liu,[e] Sara Bals,[e] Alexander V. Soldatov,[c] Gregor Mali,[b] Dirk E. De Vos *[a]

a: Centre For Membrane Separations, Adsorption, Catalysis and Spectroscopy for Sustainable Solutions (cMACS), KU Leuven, Celestijnenlaan 200F p. o. box 2461, 3001 Leuven (Belgium).

b: Department of Inorganic Chemistry and Technology, National Institute of Chemistry, Hajdrihova 19, SI-1001 Ljubljana (Slovenia).

c: The Smart Materials Research Center, Southern Federal University, Sladkova 178/24, 344090 Rostov-on-Don (Russia).

d: Southern Scientific Centre, Russian Academy of Sciences, Chekhova 41, 344006 Rostov-on-Don (Russia)

e: Electron Microscopy for Materials Science, University of Antwerp, Groenenborgerlaan 171, 2020 Antwerp (Belgium)

single-site heterogeneous catalyst, metal-organic frameworks, C-H activation, oxidative Heck reaction, palladium

ABSTRACT: Heterogeneous single-site catalysts can combine the precise active site design of organometallic complexes with the efficient recovery of solid catalysts. Based on recent progress on homogeneous thioether ligands for Pd-catalyzed C-H activation reactions, we here develop a scalable MOF-based heterogeneous single-site catalyst containing S,O-moieties that increase the catalytic activity of Pd(II) for the oxidative alkenylation of arenes. The structure of the **Pd@MOF-808-L1** catalyst was characterized in detail via solid-state nuclear magnetic resonance spectroscopy, N_2 physisorption, and high angle annular dark field scanning transmission electron microscopy, and the structure of the isolated palladium active sites could be identified by X-ray absorption spectroscopy. A turnover frequency (TOF) of 8.4 h^{-1} was reached after 1 h reaction time, which was three times higher than the TOF of standard $Pd(OAc)_2$, ranking **Pd@MOF-808-L1** among the most active heterogeneous catalysts ever reported for the non-directed oxidative alkenylation of arenes. Finally, we showed that the single-site catalyst promotes the oxidative alkenylation of a broad range of electron-rich arenes, and the applicability of this heterogeneous system was demonstrated by the gram-scale synthesis of industrially relevant products.

INTRODUCTION

Metal-catalyzed activation of C-H bonds has attracted much attention over the past decade for its potential to efficiently introduce complexity in organic molecules, without the need for prefunctionalization.[1–7] One of the most interesting C-H activation reactions is the oxidative alkenylation of arenes (also called Fujiwara-Moritani or oxidative Heck reaction), which yields vinylated aromatic motifs that are abundantly present in pharmaceuticals, natural products, agrochemicals, and other fine chemicals.[8,9] A large number of efficient oxidative alkenylation methods have been published so far, of which many employ arenes with directing groups that accelerate the rate-limiting C-H activation step by facilitating the binding of the substrate with the catalyst.[10–12] While removing the directing groups can be difficult, much progress has been made recently in developing new methods based on easily removable directing groups[13–15] and transient directing groups[16–18]. Besides directing groups, an attractive alternative strategy to enhance the activity and selectivity of the metal catalyst is the use of ancillary ligands.[19] In particular, several examples have been reported, in which the use of ligands based on amino acids,[20,21] pyridines,[22–24] pyridones,[25,26] phenanthrolines,[27,28] and 4,5-diazafluoren-9-one[29,30] increased the reaction rates of undirected C-H activation reactions and, in selected cases, even resulted in increased regioselectivities. More recently, a new class of ancillary ligands with a thioether moiety has been developed by the groups of Carrow and Fernández-Ibáñez.[31–36] These ligands greatly accelerate the palladium-catalyzed oxidative alkenylation of a broad range of simple (hetero)arenes, often even in conjunction with high regioselectivity. However, even in these state-of-the-art systems, high palladium loadings (5–10 mol%) are generally needed to achieve high yields, which impedes industrial implementation of this new synthetic strategy given the high costs associated with palladium and the strict regulations regarding trace amounts of platinum-group metals in pharmaceutical products.[37] Nevertheless, only few heterogeneous catalysts for the oxidative alkenylation of arenes have been reported so far, and the described substrate scopes are generally limited to arenes bearing directing groups (Table S10).[38–47]

Heterogeneous single-site catalysis has emerged over the past decades as an interesting tool to combine the controlled activity of organometallic catalysts with the stability and recyclability of solid catalysts, essentially bridging the gap between homogeneous and heterogeneous catalysis.[48,49] Metal-organic frameworks (MOFs), which are coordination polymers made up of inorganic secondary building units (SBUs; metal ions or clusters) and organic linkers, are a group of porous, crystalline materials that can be transformed into heterogeneous single-site catalysts.[50–54] Common strategies to imbue MOFs with structurally identical and spatially separated active sites include anchoring active transition metals on the organic linkers[55–59] or grafting

them on open coordination sites of the SBUs[60–65]. Some MOF-based systems have already been developed for C-H activation reactions, but these generally consist of pore-confined noble metal nanoparticles that catalyze only non-oxidative C-H activation reactions.[54,59] In fact, the first MOF-based catalyst for the oxidative alkenylation of arenes was only developed recently by the group of Farha, but this system suffered from low TOFs (0.06 – 0.93 h^{-1}) and converted only arenes with directing groups.[47]

Herein, we report a MOF-based heterogeneous single-site catalyst containing S,O-moieties that increase the catalytic activity of Pd(II) for the non-directed oxidative alkenylation of arenes.

RESULTS AND DISCUSSION

Synthesis of the Functionalized MOF Support

Recently, a new class of bidentate S,O-ligands was discovered, bearing a carboxylic acid group at the α position of the thioether moiety, which greatly accelerates the non-directed oxidative alkenylation of a broad range of (hetero)arenes.[33–36] Inspired by this, two new thioether carboxylic acid ligands, tetrahydrothiophene-2,5-dicarboxylic acid (**L1**) and 2-phenylthiomalonic acid (**L2**), were targeted. These ligands are designed in such a way that the carboxylic acid groups are positioned symmetrically relative to the thioether group, ensuring that an active S,O-moiety is preserved when the ligands are attached to a heterogeneous support via one of the carboxylic acid groups (Figure 1). However, **L2** was found to be prone to decarboxylation during hydrolysis of the corresponding diester (see section 3. of the Supporting Information), so the main focus was on **L1**. MOF-808 ($[Zr_6(\mu_3\text{-}O)_4(\mu_3\text{-}OH)_4(btc)_2(CH_3COO)_6]$; btc^{3-} = 1,3,5-benzenetricarboxylate) was chosen as a support to attach **L1** for several reasons: (1) the modulator ligands (formate, acetate, etc.) on the Zr_6-clusters can readily be exchanged by other ligands with carboxylic acid groups via solvent-assisted ligand exchange (SALE);[66–68] (2) the large adamantane cages with an internal pore diameter of 18.4 Å can accommodate the ligands without limiting the diffusion of reactants and products;[69,70] (3) the high oxidation state of Zr^{IV} ensures a strong bond between the Zr_6-cluster and the carboxylate group of the ligand, yielding chemically and thermally stable functionalized materials;[71,72] (4) MOF-808 can be produced cheaply on a large scale via a facile "green" synthesis route.[73] Methanol was chosen as the solvent for the SALE since it increases the mobility of the modulators on the Zr_6-clusters.[74] Subsequently, the MOFs were thoroughly washed with ethanol to remove all physisorbed ligands and dried overnight at 120 °C (see section 4. of the Supporting Information). The number of ligands per Zr_6-cluster was determined via ^1H nuclear magnetic resonance (NMR) after digesting the material in HF (Table S1). Following the optimal synthesis procedure, 2.2 **L1** ligands were on average attached to each Zr_6-cluster, with a small fraction of acetate modulators remaining. The structural formula of **MOF-808-L1** could be described as $[Zr_6(\mu_3\text{-}O)_4(\mu_3\text{-}OH)_4(btc)_2(OH)_{2.9}(H_2O)_{2.9}(CH_3COO)_{0.9}(\mathbf{L1})_{2.2}]$.

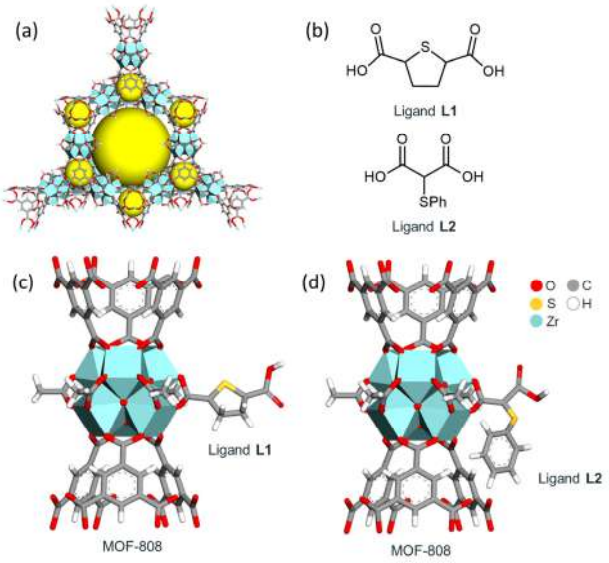

Figure 1. Structural representation of MOF-808 with its pores highlighted by yellow spheres (a), the thioether ligands **L1** and **L2** (b), **MOF-808-L1** (c) and **MOF-808-L2** (d). The Zr, O, C, H, and S atoms are represented in the structure models by turquoise, red, gray, white, and yellow sticks, respectively.

Further investigation of the spatial organization of **MOF-808-L1** was undertaken via solid-state NMR experiments to establish the position of **L1** in the framework and whether **L1** is homogeneously distributed over the MOF-808 crystals rather than being segregated into domains. First, a two-dimensional ^1H–^{13}C cross-polarization heteronuclear correlation (CP-HETCOR) NMR spectrum was recorded to correctly assign the signals of the ^1H and ^{13}C magic angle spinning (MAS) NMR spectra (Figure 2a and Figure S3). Notably, two signals can be observed for the COO nuclei of **L1** (192 ppm and 178 ppm), implying that one COO group is attached to the Zr_6-cluster, and the other one is dangling in the pore. After identification of all relevant resonances, ^1H–^1H double-quantum/single-quantum (DQ-SQ) MAS NMR experiments were performed to probe short-distance relations. For unmodified MOF-808, strong off-diagonal cross-peaks can be observed between the aromatic protons of btc^{3-} (8.9 ppm) and the protons of the acetate modulators (1.6 ppm) (Figure 2b; green line), and between the aromatic protons of btc^{3-} (8.9 ppm) and the H_2O-groups of the defect sites (2.2 ppm) and the μ_3-OH groups (0.8 ppm) (Figure 2b; blue lines), which implies that these species are in close proximity of the btc^{3-} linkers. This is evident since all of them are located at the Zr_6-cluster. Interestingly, a similar cross-peak can be noted for **MOF-808-L1** between the aromatic protons of btc^{3-} (8.9 ppm) and the aliphatic protons of **L1** (3.8 ppm and 2.4 ppm) (Figure 2c; orange lines), indicating that **L1** is also located on the Zr_6-clusters. In addition, ^1H spin-diffusion experiments of MOF-808 and **MOF-808-L1** were performed, which probe the rate of polarization transfer between chemically distinct protons (protons of btc^{3-} linkers, **L1** ligands, acetate modulators) to evaluate long-distance correlations between these species. When two species are intimately mixed, the average rate of

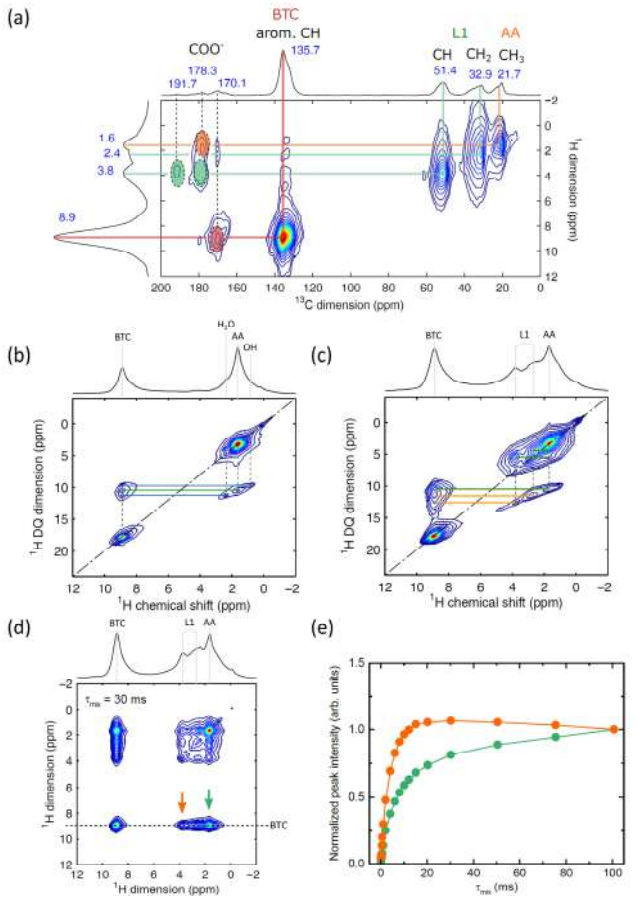

Figure 2. (a) Two-dimensional $^{1}H–^{13}C$ CP-HETCOR MAS NMR spectrum of **MOF-808-L1**. $^{1}H–^{1}H$ DQ-SQ MAS NMR spectrum of MOF-808 (b) and **MOF-808-L1** (c). The off-diagonal cross-peaks between the protons of btc^{3-} and the protons of the acetate (AA) modulators, the protons of btc^{3-} and the protons of the μ_3-OH and H_2O groups, and the protons of btc^{3-} and the protons of **L1** are highlighted by green, blue and orange lines, respectively. (d) ^{1}H spin-diffusion spectrum of **MOF-808-L1**. The off-diagonal cross-peaks between the protons of btc^{3-} and the protons of the acetate modulators, and the protons of btc^{3-} and the protons of **L1** are highlighted by green and orange arrows, respectively. (e) ^{1}H spin-diffusion curves of **MOF-808-L1** based on the off-diagonal cross-peaks between the protons of btc^{3-} and the protons of the acetate modulators (green), and the protons of btc^{3-} and the protons of **L1** (orange) as a function of the mixing time.

polarization transfer will be faster than when they are segregated into domains. The off-diagonal cross-peaks between the aromatic protons of btc^{3-} (8.9 ppm) and the aliphatic protons of **L1** (3.8 ppm and 2.4 ppm) reveal that there is polarization transfer between these protons and that both species are in proximity to each other (Figure 2d). Moreover, the spin-diffusion curves, which are constructed by measuring the volumes of the cross-peaks between the aromatic protons of btc^{3-} and the aliphatic protons of **L1** (Figure 2e; orange line) or acetate (Figure 2e; green line) as a function of the mixing time, indicate that the distribution of **L1** in the MOF-808 crystals is similar to or even more homogeneous than the distribution of the acetate modulators since the initial part of the spin-diffusion curve is steeper, and a plateau is quickly reached.[75]

More information on how **L1** is incorporated into the framework of MOF-808 was also provided by N_2 sorption measurements. As expected, a decrease in Brunauer-Emmett-Teller (BET) surface area from 2380 m^2/g for MOF-808 to 1460 m^2/g for **MOF-808-L1** could be observed. Furthermore, micropore size distributions show that the average internal pore diameter of the large adamantane cage decreases from 18.4 Å to 14.9 Å after **L1** incorporation, while the size of the small tetrahedral cages remains unchanged (Figure S6). This shows that **L1** is indeed located in the large adamantane cage, ensuring easy access to its S,O-moiety. Moreover, the micropore size distribution of the large adamantane cage is similarly narrow before and after ligand attachment, which again indicates that **L1** is homogeneously distributed over all large cages.

Incorporation of Pd(II) into MOF-808-L1

The obtained **MOF-808-L1** material was generally loaded with an equimolar amount of $Pd(OAc)_2$ relative to **L1** in dichloromethane (DCM) (see section 9. of the Supporting Information). After 24 h, the solution became colorless, and a bright orange powder was obtained (Figure S7), indicating that all Pd(II) species migrated to the functionalized MOF support. After removing DCM under vacuum, the active catalyst (**Pd@MOF-808-L1**) was obtained and stored under argon atmosphere until further use.

Since only Pd(II) species, in contrast to Pd(0), can catalyze the oxidative alkenylation reaction, the oxidation state of Pd in the preloaded material is of paramount importance for its catalytic activity. High angle annular dark field scanning transmission electron microscopy (HAADF-STEM) images of the preloaded material in combination with energy dispersive X-ray spectroscopy (EDX) confirmed that the Pd(II) centers were homogeneously dispersed over the MOF material and no evidence of Pd(0) nanoparticles could be found in the preloaded catalyst (Figure S12), which is in line with its bright orange color. The absence of Pd(0) in the preloaded material was further evidenced by analysis of the X-ray absorption near edge structure (XANES) of the Pd-loaded material, which showed that the Pd centers occur solely as Pd(II) species (Figure S9). Moreover, the absence of features originating from Pd–Pd interactions in the Fourier transformed extended X-ray absorption fine structure (FT-EXAFS) spectrum of the preloaded material excludes the presence of Pd(0) nanoparticles and confirms that the Pd(II) centers are distributed over the MOF material as isolated active sites (Figure 3a).

In-depth analysis of the FT-EXAFS spectra of the Pd(II)-loaded materials also provided information on how the supported Pd(II) centers interact with the **L1** ligands. A distinct feature originating from Pd–S interactions appears after preloading, confirming that the Pd(II) species are indeed located in the vicinity of the S,O-moieties of the thioether ligands. Furthermore, the local environment of the isolated active sites could be identified based on the FT-EXAFS data (Figure 3b). A good fit was obtained between the measured spectrum of **Pd@MOF-808-L1** and the simulated spectrum

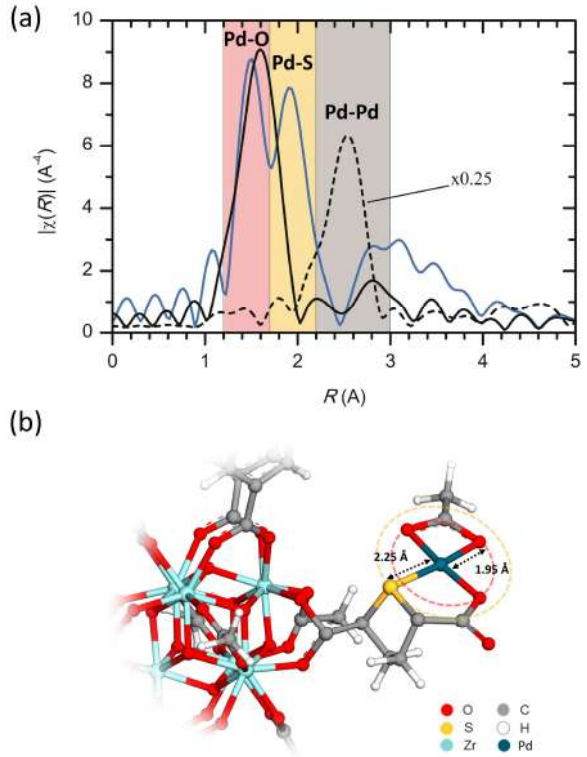

Figure 3. (a) The magnitude of the phase-uncorrected Fourier transformed experimental k^3-weighted Pd *K*-edge EXAFS spectra of $Pd(OAc)_2$ (black, solid line), Pd(0) nanopowder (black, dashed line), and preloaded **Pd@MOF-808-L1** (blue line), in R-space. Pd–O, Pd–S and Pd–Pd contributions are highlighted by a red, yellow and gray background, respectively. (b) Structural representation of the fitted model of the isolated Pd(II) active site of **Pd@MOF-808-L1**. The Zr, O, C, H, S and Pd atoms are represented in the structure model by turquoise, red, gray, white, yellow and dark blue spheres, respectively. The first and second shells are indicated by red and yellow dashed circles, respectively.

of the first two shells of the proposed structure with fitted interatomic Pd–O and Pd–S distances of 1.95 ± 0.01 Å and 2.28 ± 0.02 Å, respectively (Figure S11).

Pd(II)-catalyzed oxidative alkenylation of arenes

The performance of the **Pd@MOF-808-L1** material as a single-site heterogeneous catalyst for the Pd(II)-catalyzed oxidative alkenylation of arenes was tested by employing 2,6-dimethylanisole and *n*-butyl acrylate as model substrates, *tert*-butyl peroxybenzoate (TBPB) as oxidant, and performing the reaction under optimized reaction conditions (see sections 10. and 11. of the Supporting Information). A significantly higher yield (62%) was obtained when 5 mol% **Pd@MOF-808-L1** was used as catalyst compared to standard $Pd(OAc)_2$ and Pd(II)-loaded unmodified MOF-808 (22% and 25%, respectively) (Table 1, entries 1-3), confirming our hypothesis that the MOF-supported S,O-moieties increase the catalytic activity of Pd(II). Compared to the reaction with preloaded **Pd@MOF-808-L1**, a similar high yield was obtained when 5 mol% $Pd(OAc)_2$ and 5 mol% **MOF-808-L1** were added separately (Table 1, entries 3 and

Table 1. Performance of the Catalyst for the Oxidative Alkenylation of 2,6-Dimethylanisole with *n*-Butyl Acrylate.[a]

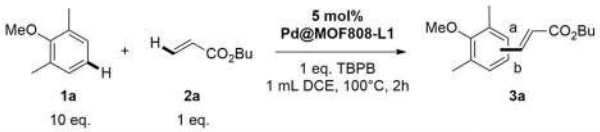

Entry	Catalyst	Yield **3a** (%)[b]	Regioselectivity (a:b)
1	$Pd(OAc)_2$	22	1:1.5
2	Pd@MOF-808	25	1:1.2
3	Pd@MOF-808-L1	63	1:1.8
4	$Pd(OAc)_2$ + MOF-808-L1	62	1:1.8
5	Pd@MOF-808-L1[c]	72	1:1.9
6	Pd@NU-1000-L1	58	1:1.6
7	$Pd(OAc)_2$ + L1	12	1:1.4

[a]Reaction conditions: **1a** (2.5 mmol), **2a** (0.25 mmol), TBPB (0.25 mmol), **Pd@MOF-808-L1** (5 mol%) and DCE (1 mL) at 100 °C for 2 h. [b]Yield was determined by GC-FID with hexadecane as internal standard. [c]10 mol% **Pd@MOF-808-L1**.

4), implying that the S,O-moieties have a strong affinity for Pd(II) to readily form the active single-site catalyst in situ. Moreover, the catalytic results were more consistent when **MOF-808-L1** was loaded in situ with $Pd(OAc)_2$ (Table S2). This suggests that a more robust S,O-supported Pd(II) catalyst is generated by loading **MOF-808-L1** in situ with Pd(II). By increasing the amount of catalyst to 10 mol%, the yield further increased to 72% (Table 1, entry 5). The generality of our approach was demonstrated by incorporating ligand **L1** into the framework of NU-1000 ($[Zr_6(\mu_3\text{-}O)_4(\mu_3\text{-}OH)_4(OH)_4(H_2O)_4$ (tbapy)$_2$]; tbapy^{4-} = 1,3,6,8-tetrakis(*p*-benzoate)pyrene), which is another stable Zr-MOF with large pores that can be modified with carboxylate ligands (see section 4.2. of the Supporting Information).[66] The obtained yield with **Pd@NU-1000-L1** as catalyst (58%) was just slightly lower than with **Pd@MOF-808-L1** (63%) and still significantly higher than when no thioether ligands were present (22%) (Table 1, entries 1 and 6). The small drop in yield could suggest slightly inferior accessibility or distribution of **L1** on NU-1000 compared to MOF-808, although more extensive characterization of **Pd@NU-1000-L1** is needed to confirm this. A pale yellow precipitate was formed after several minutes when **L1** was added as a homogeneous ligand to $Pd(OAc)_2$, and the alkenylated product was only formed in 12% yield, indicating that the resulting catalyst complex was not very soluble in 1,2-dichloroethane (DCE) (Table 1, entry 7). Nevertheless, the intrinsic property of the S,O-moiety of **L1** to increase the catalytic activity of Pd(II) was proven by performing the reaction in acetic acid (Table S7).

Having established that the use of our single-site heterogeneous catalyst resulted in higher yields compared to standard $Pd(OAc)_2$, the yield was monitored over time to ex-

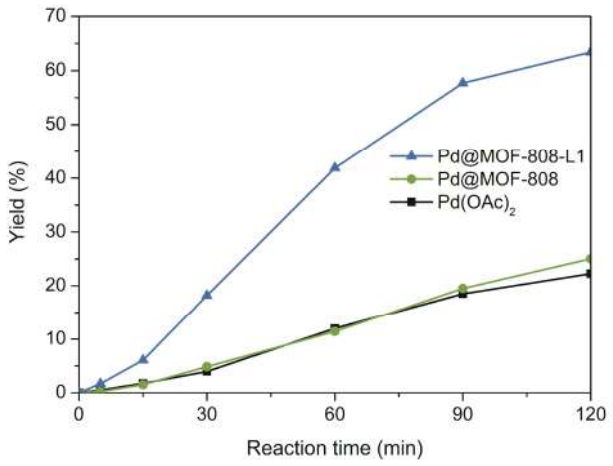

Figure 4. Kinetic profile of the oxidative alkenylation of 2,6-dimethylanisole with *n*-butyl acrylate catalyzed by $Pd(OAc)_2$ (black), Pd@MOF-808 (green) and **Pd@MOF-808-L1** (blue). The yield is the sum of both isomers.

amine the origin of this increase in yield (Figure 4). The kinetic profiles clearly show that already from the onset of the reaction, higher yields are obtained with Pd@MOF-808-L1 than with homogeneous $Pd(OAc)_2$, implying that the **MOF-808-L1** material increases the catalytic activity of the Pd(II) centers. Moreover, the rate of the reaction with **Pd@MOF-808-L1** is also considerably higher than the rate of the reaction with Pd@MOF-808, confirming that the increase in activity originates from the tailor-made S,O-moieties. After 1 h, a TOF of 8.4 h^{-1} was achieved, ranking **Pd@MOF-808-L1** among the most active heterogeneous catalysts ever reported for the non-directed oxidative alkenylation of arenes.

Catalyst stability

The stability of the single-site MOF catalysts was evaluated by comparing the X-ray diffraction patterns before and after the reaction (Figures S1 and S2). No significant decrease in crystallinity could be observed, highlighting the high intrinsic thermal, mechanical, and chemical stability of the MOF-808 support. More information on the nature of the active Pd(II) centers of the spent catalyst was obtained via XANES (Figure S9) and EXAFS (Figure S10) analysis. After 1 h reaction time, the intensity of the Pd–O interactions remains the same as in the preloaded material, but the contribution of the Pd–S interactions decreases slightly, which might suggest that several Pd species are present. Furthermore, no contribution from Pd–Pd interactions can be observed after 1 h, indicating that deactivated Pd(0) nanoparticles are not yet formed. Only after 2 h of reaction time, the catalyst starts to deactivate, and a Pd–Pd signal appears, which is in agreement with the kinetic profile. The formation of Pd(0) nanoparticles was further evidenced by HAADF-STEM images of the spent catalyst. Although absent in the sample after 1 h reaction time, Pd(0) nanoparticles could be observed in the sample after 2 h (Figure 5 and Figures S12-14). Interestingly, the sulfur-containing **L1** ligands were still homogeneously dispersed over the crystals, indicating that **L1** remained firmly attached to the Zr_6-cluster

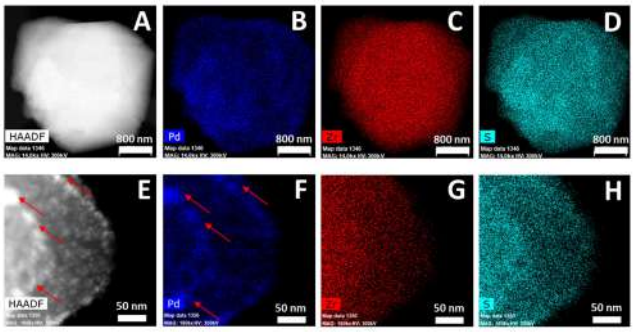

Figure 5. HAADF-STEM images of **Pd@MOF-808-L1** after 1 h (A-D) and 2 h (E-H) reaction time in combination with EDX. Pd mapping is displayed in blue, Zr in red, and S in cyan. Pd(0) nanoparticles are indicated by red arrows.

under reaction conditions. In fact, liquid ^{1}H NMR analysis of the spent catalysts after digestion revealed that only 4% of the **L1** ligands were leached (Table S9), and ^{13}C MAS NMR measurements indicated that the thioether moieties did not get oxidized during the reaction (Figure S4). Furthermore, palladium leaching was determined by inductively coupled plasma optical emission spectrometry (ICP-OES) (Table S8). The palladium content in the reaction solution could be minimized to 11 ppm, which corresponds to only 1.4% leaching, implying that the expensive palladium can efficiently be recovered after the reaction. The heterogeneity of the catalytic system was further evidenced by a hot filtration test (Figure S8). Nevertheless, the activity of the catalyst could not be retained upon recycling, which indicates that inactive Pd species were formed that could not readily be reactivated by TBPB. A control experiment with Pd(0) powder (particle size: 350 – 800 nm) furnished the product in only trace amounts (Table S7), indicating that catalyst deactivation can indeed be the result of Pd(0) nanoparticle formation. Moreover, similar recyclability issues have also been observed for other heterogeneous catalysts for this reaction.[47]

Substrate scope and scalability

Besides the model substrates 2,6-dimethylanisole and *n*-butyl acrylate, several other arenes and alkenes were tested to investigate the scope of the catalytic system (Table 2). Arenes bearing electron-donating groups could be converted into the respective alkenylated products **3a-e** in good to excellent yields. In particular, 2,6-dimethylphenol could efficiently be alkenylated with merely 1 mol% catalyst, and a turnover number (TON) of 49 was reached. However, it should be noted that hydroxyl and methoxy substituents can function, albeit weakly, as directing groups for C-H cleavage at the *ortho* positions.[12,76] Besides electron-rich arenes, the oxidative C-H alkenylation of aromatics with alkyl substituents was also studied. The reaction with *o*-xylene furnished product **3f** in 34% yield and even lower yields were achieved using toluene, *p*- and *m*-xylene (**3g**: 22%, **3h**: 25% and **3i**: 31%, respectively), indicating that especially electron-rich arenes are efficiently converted by our developed single-site heterogeneous catalyst. Consequently, we also tested several electron-rich heteroarenes

Table 2. Substrate Scope[a]

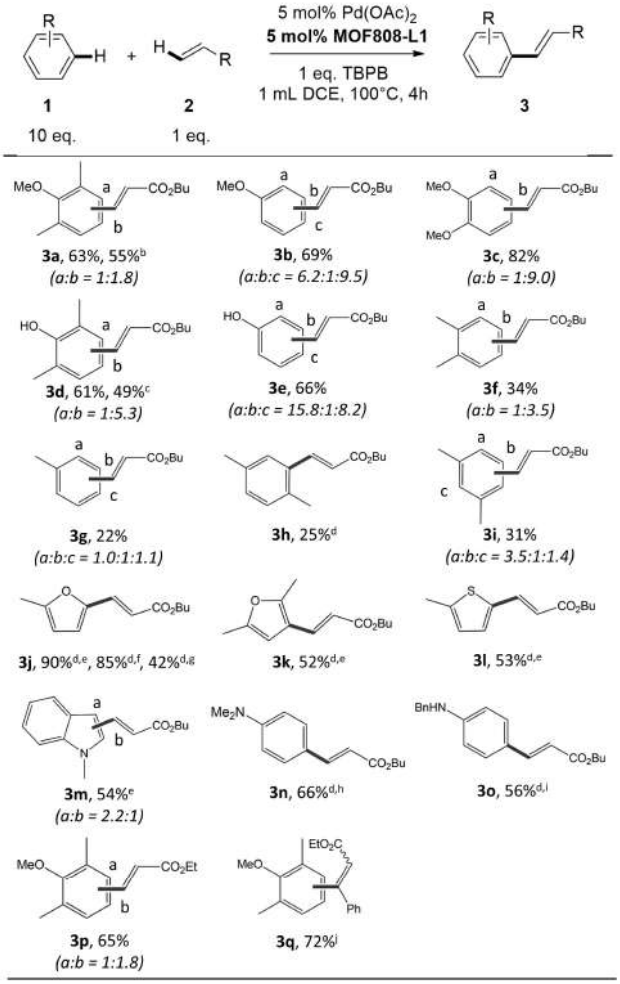

[a]Standard reaction conditions: **1** (2.5 mmol), **2** (0.25 mmol), TBPB (0.25 mmol), $Pd(OAc)_2$ (5 mol%), **MOF-808-L1** (5 mol%) and DCE (1 mL) at 100 °C for 4 h. Products were analyzed by ^1H NMR and/or GC-MS. Yield was determined by GC-FID with hexadecane as internal standard. [b]2.5 mol% $Pd(OAc)_2$, 2.5 mol% **MOF-808-L1** and 3 h. [c]1 mol% $Pd(OAc)_2$, 1 mol% **MOF-808-L1** and 24 h. [d]only one regioisomer was formed. [e]**1** (0.5 mmol), 70 °C. [f]**1** (0.5 mmol), 2.5 mol% $Pd(OAc)_2$, 2.5 mol% **MOF-808-L1**, 70 °C and 6 h. [g]**1** (0.5 mmol), 1 mol% $Pd(OAc)_2$, 1 mol% **MOF-808-L1**, 70 °C and 6 h. [h]**1** (0.25 mmol), **2** (0.375 mmol), 10 mol% $Pd(OAc)_2$, 10 mol% **MOF-808-L1**, 40 °C and 17 h. [i]**1** (0.375 mmol), 10 mol% $Pd(OAc)_2$, 10 mol% **MOF-808-L1**, 80 °C and 17 h. [j]sum of all regio- and *cis/trans*-isomers.

as substrate. The alkenylation product of 2-methylfuran **3j** could be obtained in 90% yield. Even with only 2.5 mol% catalyst, product **3j** was formed in 85% yield. When 2,5-dimethylfuran, 2-methylthiophene, and 1-methylindole were employed as substrates, products **3k**, **3l**, and **3m** were formed in 52%, 53% and 54% yield, respectively. Recent work by the group of Fernández-Ibáñez showed that palladium ligated by thioether ligands with an S,O-moiety could efficiently catalyze the C-H alkenylation of aniline derivatives with high *para*-selectivity.[36] In agreement with these results, reactions with *N,N*-dimethylaniline and *N*-benzylaniline furnished the alkenylation products in high yields (**3n**: 66% and **3o**: 56%, respectively) and with complete

Table 3. Gram-Scale Synthesis of Industrially Relevant Coupling Products via the Oxidative Alkenylation of Arenes[a]

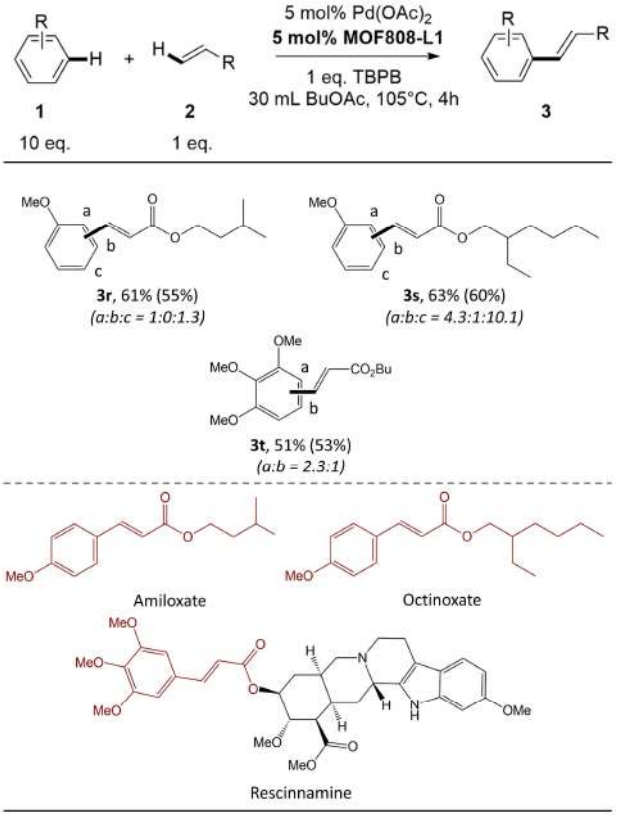

[a]Reaction conditions: **1** (75 mmol), **2** (7.5 mmol), TBPB (7.5 mmol), $Pd(OAc)_2$ (5 mol%), **MOF-808-L1** (5 mol%) and butyl acetate (30 mL) at 105 °C for 4 h. Products were analyzed by ^1H NMR and GC-FID/GC-MS. Yield was determined by GC-FID with hexadecane as internal standard and the isolated yield is displayed between brackets.

para-selectivity. Finally, when ethyl acrylate and ethyl cinnamate were utilized as alkenes, the respective products **3p** (65%), **3q** (72%) were obtained in high yields. Overall, a broad range of electron-rich arenes could be converted by this new single-site catalyst in decent to good yields, but it should be noted that for many cases, higher yields and especially better regioselectivities could be attained using specialized homogeneous systems.[24,26,31,33,36]

Since both MOF-808 and **L1** are synthesized from cheap starting reagents, their synthesis is easily upscaled to a multi-gram scale, and an inexpensive oxidant, TBPB, is used for the oxidative alkenylation reaction (instead of e.g. expensive Ag-salts), the performance of the catalyst was also evaluated in a gram-scale reaction (see section 10.3. of the Supporting Information). To the best of our knowledge, a heterogeneous system for the oxidative alkenylation of arenes without directing groups has not yet been tested on such a scale. Moreover, industrially relevant substrates were selected to demonstrate the significance of the developed catalyst system for the fine chemical and pharmaceutical industry (Table 3). Products **3r** and **3s**, which resemble the molecular structure of the widely used sunscreen agents Amiloxate and Octinoxate, could be obtained in good yields.

Furthermore, product **3t**, which can be converted into the antihypertensive drug Rescinnamine in just one additional step, was also formed in a reasonable yield. However, the regioselectivity for the desired isomer was, in all cases, moderate to low, highlighting one of the key issues of C-H activation reactions compared to traditional cross-coupling reactions. Nevertheless, given the facile recovery of the precious palladium, the limited noble metal leaching, the scalability of the reactions, and the inexpensive nature of the coupling reagents, oxidant and catalyst system, one can expect that the industrial relevance of such heterogeneous catalyst systems for the fine chemical and pharmaceutical industry will only increase in the future.

CONCLUSIONS

In this work, we have developed heterogeneous single-site MOF catalysts for the oxidative alkenylation of arenes based on the excellent results that were recently obtained using homogeneous thioether ligands for palladium-catalyzed C-H activation reactions. MOF-808 was selected as catalyst support, given its flexibility to reliably incorporate carboxylate ligands in a well-defined way. Following the optimal synthesis procedure, 2.2 **L1** ligands were on average attached to each Zr_6-cluster, and a combination of several solid-state NMR experiments and N_2 physisorption measurements revealed that the **L1** ligands were homogeneously distributed over the large adamantane cages of MOF-808. Moreover, it was shown that the MOF-supported S,O-moieties increase the catalytic activity of Pd(II). A TOF of 8.4 h^{-1} was reached after 1 h reaction time, which was a threefold higher than the TOF of standard $Pd(OAc)_2$. Although the rates are still below those of the most active homogeneous systems, this ranks **Pd@MOF-808-L1** among the most active heterogeneous catalysts ever reported for the non-directed oxidative alkenylation of arenes. The structure of the isolated palladium active sites could be identified via EXAFS analysis, and the stability of the catalyst was monitored via XANES, EXAFS, and HAADF-STEM. Finally, we showed that the catalyst promotes the oxidative alkenylation of a broad range of electron-rich arenes, and the applicability of this new heterogeneous system was demonstrated by the gram-scale synthesis of industrially relevant products. Nevertheless, significant progress on the activity, stability, and recyclability of this new MOF-based catalyst is needed to reach industrially relevant TONs and TOFs. Overall, this work highlights that inexpensive single-site MOF catalysts can combine the precise active site design of state-of-the-art organometallic complexes with the facile recovery of solid catalysts and limited noble metal leaching. These results can provide insights into the design and characterization of new single-site heterogeneous catalysts, and significant progress in this field is expected in the coming decade.

AUTHOR INFORMATION

Corresponding Author

* E-mail for D.E.D.V.: dirk.devos@kuleuven.be.

ORCID

Niels Van Velthoven: 0000-0003-3224-0239

Mickaël Henrion: 0000-0001-8682-5182

Andraž Krajnc: 0000-0003-2249-602X

Aram Bugaev: 0000-0001-8273-2560

Pei Liu: 0000-0003-4843-8565

Sara Bals: 0000-0002-4249-8017

Alexander Soldatov: 0000-0001-8411-0546

Gregor Mali: 0000-0002-9012-2495

Dirk De Vos: 0000-0003-0490-9652

Author Contributions

The manuscript was written through the contributions of all authors. All authors have given approval to the final version of the manuscript.

Notes

The authors declare no competing financial interest.

ASSOCIATED CONTENT

Supporting Information. Detailed experimental procedures, optimization of the reaction conditions, and additional characterization data (PDF). This material is available free of charge via the Internet at http://pubs.acs.org.

ACKNOWLEDGMENT

The research leading to these results has received funding from the NMBP-01-2016 Program of the European Union's Horizon 2020 Framework Program H2020/2014-2020/ under grant agreement n° [720996]. N. V. V. and D. E. D. V. thank the FWO for funding (1S32917N and G0F2320N). D. E. D. V. is grateful for KU Leuven's support in the frame of the CASAS Metusalem project and a C3 type project. A. K. and G. M. acknowledge the financial support from the Slovenian Research Agency (research core funding No. P1-0021 and project No. N1-0079). A.L.B and A.V.S. acknowledge Russian Science Foundation grant # 20-43-01015 for financial support. We thank Alexander Trigub and Alexey Veligzhanin for their support during the beamtime at Kurchatov Institute. We are indebted to Elizaveta Kamyshova and Anna Pnevskaya for their valuable help during EXAFS measurements. P.L. and S.B. thank European Research Council for the ERC Consolidator Grant 815128, REALNANO. Kassem Amro and Guillaume Gracy from Sikemia are gratefully acknowledged for providing **L1**.

ABBREVIATIONS

TOF, turnover frequency; MOFs, Metal-organic frameworks; SBUs, secondary building units; btc^{3-}, 1,3,5-benzenetricarboxylate; SALE, solvent-assisted ligand exchange; NMR, nuclear magnetic resonance; CP-HETCOR, cross-polarization heteronuclear correlation; MAS, magic angle spinning; DQ-SQ, double-quantum/single-quantum; BET, Brunauer-Emmett-Teller; DCM, dichloromethane; HAADF-STEM, High angle annular dark field scanning transmission electron microscopy; EDX, energy dispersive X-ray spectroscopy; XANES, X-ray absorption near edge structure; FT-EXAFS, Fourier transformed extended X-ray absorption fine structure; TBPB, *tert*-butyl peroxybenzoate; $tbapy^{4-}$, 1,3,6,8-tetrakis(*p*-benzoate)pyrene; DCE, 1,2-dichloroethane; ICP-OES, inductively coupled plasma optical emission spectrometry; TON, turnover number.

REFERENCES

(1) Yamaguchi, J.; Yamaguchi, A. D.; Itami, K. C-H Bond

Functionalization: Emerging Synthetic Tools for Natural Products and Pharmaceuticals. *Angew. Chem., Int. Ed.* **2012**, *51*, 8960–9009.

(2) Wedi, P.; van Gemmeren, M. Arene-Limited Nondirected C–H Activation of Arenes. *Angew. Chem., Int. Ed.* **2018**, *57*, 13016–13027.

(3) Park, Y.; Kim, Y.; Chang, S. Transition Metal-Catalyzed C-H Amination: Scope, Mechanism, and Applications. *Chem. Rev.* **2017**, *117*, 9247–9301.

(4) Yang, Y.; Lan, J.; You, J. Oxidative C-H/C-H Coupling Reactions between Two (Hetero)Arenes. *Chem. Rev.* **2017**, *117*, 8787–8863.

(5) Hartwig, J. F. Evolution of C-H Bond Functionalization from Methane to Methodology. *J. Am. Chem. Soc.* **2016**, *138*, 2–24.

(6) Girard, S. A.; Knauber, T.; Li, C. J. The Cross-Dehydrogenative Coupling of Csp3 -H Bonds: A Versatile Strategy for C-C Bond Formations. *Angew. Chem., Int. Ed.* **2014**, *53*, 74–100.

(7) Gensch, T.; Hopkinson, M. N.; Glorius, F.; Wencel-Delord, J. Mild Metal-Catalyzed C-H Activation: Examples and Concepts. *Chem. Soc. Rev.* **2016**, *45*, 2900–2936.

(8) Le Bras, J.; Muzart, J. Intermolecular Dehydrogenative Heck Reactions. *Chem. Rev.* **2011**, *111*, 1170–1214.

(9) Zhou, L.; Lu, W. Towards Ideal Synthesis: Alkenylation of Aryl C-H Bonds by a Fujiwara-Moritani Reaction. *Chem. - Eur. J.* **2014**, *20*, 634–642.

(10) Lyons, T. W.; Sanford, M. S. Palladium-Catalyzed Ligand-Directed C-H Functionalization Reactions. *Chem. Rev.* **2010**, *110*, 1147–1169.

(11) Kozhushkov, S. I.; Ackermann, L. Ruthenium-Catalyzed Direct Oxidative Alkenylation of Arenes through Twofold C-H Bond Functionalization. *Chem. Sci.* **2013**, *4*, 886–896.

(12) Sambiagio, C.; Schönbauer, D.; Blieck, R.; Dao-Huy, T.; Pototschnig, G.; Schaaf, P.; Wiesinger, T.; Zia, M. F.; Wencel-Delord, J.; Besset, T.; Maes, B. U. W.; Schnürch, M. A Comprehensive Overview of Directing Groups Applied in Metal-Catalysed C-H Functionalisation Chemistry. *Chem. Soc. Rev.* **2018**, *47*, 6603–6743.

(13) Wang, C.; Huang, Y. Expanding Structural Diversity; Removable and Manipulable Directing Groups for C-H Activation. *Synlett* **2013**, *24*, 145–149.

(14) Ma, W.; Gandeepan, P.; Li, J.; Ackermann, L. Recent Advances in Positional-Selective Alkenylations: Removable Guidance for Twofold C-H Activation. *Org. Chem. Front.* **2017**, *4*, 1435–1467.

(15) Rej, S.; Chatani, N. Rhodium-Catalyzed C(Sp2)- or C(Sp3)–H Bond Functionalization Assisted by Removable Directing Groups. *Angew. Chem., Int. Ed.* **2019**, *58*, 8304–8329.

(16) Zhao, Q.; Poisson, T.; Pannecoucke, X.; Besset, T. The Transient Directing Group Strategy: A New Trend in Transition-Metal-Catalyzed C-H Bond Functionalization. *Synth.* **2017**, *49*, 4808–4826.

(17) Bhattacharya, T.; Pimparkar, S.; Maiti, D. Combining Transition Metals and Transient Directing Groups for C-H Functionalizations. *RSC Adv.* **2018**, *8*, 19456–19464.

(18) Gandeepan, P.; Ackermann, L. Transient Directing Groups for Transformative C–H Activation by Synergistic Metal Catalysis. *Chem* **2018**, *4*, 199–222.

(19) Engle, K. M.; Yu, J. Q. Developing Ligands for Palladium(II)-Catalyzed C-H Functionalization: Intimate Dialogue between Ligand and Substrate. *J. Org. Chem.* **2013**, *78*, 8927–8955.

(20) Engle, K. M.; Wang, D. H.; Yu, J. Q. Ligand-Accelerated C-H Activation Reactions: Evidence for a Switch of Mechanism. *J. Am. Chem. Soc.* **2010**, *132*, 14137–14151.

(21) Wang, D. H.; Engle, K. M.; Shi, B. F.; Yu, J. Q. Ligand-Enabled Reactivity and Selectivity in a Synthetically Versatile Aryl C-H Olefination. *Science* **2010**, *327*, 315–319.

(22) Zhang, Y.; Shi, B.; Yu, J. Pd(II)-Catalyzed Olefination of Electron-Deficient Arenes Using 2,6-Dialkylpyridine Ligands. **2009**, *131*, 5072–5074.

(23) Kubota, A.; Emmert, M. H.; Sanford, M. S. Pyridine Ligands as Promoters in PdII/0-Catalyzed C-H Olefination Reactions. *Org. Lett.* **2012**, *14*, 1760–1763.

(24) Chen, H.; Wedi, P.; Meyer, T.; Tavakoli, G.; van Gemmeren, M. Dual Ligand-Enabled Nondirected C–H Olefination of Arenes. *Angew. Chem., Int. Ed.* **2018**, *57*, 2497–2501.

(25) Wang, P.; Farmer, M. E.; Huo, X.; Jain, P.; Shen, P.-X.; Ishoey, M.; Bradner, J. E.; Wisniewski, S. R.; Eastgate, M. D.; Yu, J.-Q. Ligand-Promoted Meta-C–H Arylation of Anilines, Phenols, and Heterocycles. *J. Am. Chem. Soc.* **2016**, *138*, 9269–9276.

(26) Wang, P.; Verma, P.; Xia, G.; Shi, J.; Qiao, J. X.; Tao, S.; Cheng, P. T. W.; Poss, M. A.; Farmer, M. E.; Yeung, K. S.; Yu, J. Q. Ligand-Accelerated Non-Directed C-H Functionalization of Arenes. *Nature* **2017**, *551*, 489–493.

(27) Ye, M.; Gao, G. L.; Yu, J. Q. Ligand-Promoted C-3 Selective C-H Olefination of Pyridines with Pd Catalysts. *J. Am. Chem. Soc.* **2011**, *133*, 6964–6967.

(28) Gao, G. L.; Xia, W.; Jain, P.; Yu, J. Q. Pd(II)-Catalyzed C3-Selective Arylation of Pyridine with (Hetero)Arenes. *Org. Lett.* **2016**, *18*, 744–747.

(29) Campbell, A. N.; Meyer, E. B.; Stahl, S. S. Regiocontrolled Aerobic Oxidative Coupling of Indoles and Benzene Using Pd Catalysts with 4,5-Diazafluorene Ligands. *Chem. Commun.* **2011**, *47*, 10257–10259.

(30) Vasseur, A.; Laugel, C.; Harakat, D.; Muzart, J.; Bras, J. Le. Ligand-Promoted Reactivity of Alkenes in Dehydrogenative Heck Reactions of Furans and Thiophenes. *Eur. J. Org. Chem.* **2015**, *2015*, 944–948.

(31) Gorsline, B. J.; Wang, L.; Ren, P.; Carrow, B. P. C-H Alkenylation of Heteroarenes: Mechanism, Rate, and Selectivity Changes Enabled by Thioether Ligands. *J. Am. Chem. Soc.* **2017**, *139*, 9605–9614.

(32) Wang, L.; Carrow, B. P. Oligothiophene Synthesis by a General C-H Activation Mechanism: Electrophilic Concerted Metalation-Deprotonation (ECMD). *ACS Catal.* **2019**, *9*, 6821–6836.

(33) Naksomboon, K.; Valderas, C.; Gómez-Martínez, M.; Álvarez-Casao, Y.; Fernández-Ibáñez, M. Á. S,O-Ligand-Promoted Palladium-Catalyzed C–H Functionalization Reactions of Nondirected Arenes. *ACS Catal.* **2017**, *7*, 6342–6346.

(34) Naksomboon, K.; Álvarez-Casao, Y.; Uiterweerd, M.; Westerveld, N.; Maciá, B.; Fernández-Ibáñez, M. Á. S,O-Ligand-Promoted Palladium-Catalyzed C–H Olefination of Arenes with Allylic Substrates. *Tetrahedron Lett.* **2018**, *59*, 379–382.

(35) Álvarez-Casao, Y.; Fernández-Ibáñez, M. Á. S,O-Ligand-Promoted Pd-Catalyzed C–H Olefination of Thiophenes. *Eur. J. Org. Chem.* **2019**, *2019*, 1842–1845.

(36) Naksomboon, K.; Poater, J.; Bickelhaupt, F. M.; Fernández-Ibáñez, M. Á. Para-Selective C–H Olefination of Aniline Derivatives via Pd/S,O-Ligand Catalysis. *J. Am. Chem. Soc.* **2019**, *141*, 6719–6725.

(37) Hayler, J. D.; Leahy, D. K.; Simmons, E. M. A Pharmaceutical Industry Perspective on Sustainable Metal Catalysis. *Organometallics* **2019**, *38*, 36–46.

(38) Hájek, J.; Dams, M.; Detrembleur, C.; Jérôme, R.; Jacobs, P. A.; De Vos, D. E. Heterogeneous Alkenylation of Aromatics under Oxygen. *Catal. Commun.* **2007**, *8*, 1047–1051.

(39) Chng, L. L.; Zhang, J.; Yang, J.; Amoura, M.; Ying, J. Y. C-C Bond Formation via C-H Activation and C-N Bond Formation via Oxidative Amination Catalyzed by Palladium-Polyoxometalate Nanomaterials Using Dioxygen as the Terminal Oxidant. *Adv. Synth. Catal.* **2011**, *353*, 2988–2998.

(40) Duan, H.; Li, M.; Zhang, G.; Gallagher, J. R.; Huang, Z.; Sun, Y.; Luo, Z.; Chen, H.; Miller, J. T.; Zou, R.; Lei, A.; Zhao, Y. Single-Site Palladium(II) Catalyst for Oxidative Heck Reaction: Catalytic Performance and Kinetic Investigations. *ACS Catal.* **2015**, *5*, 3752–3759.

(41) Huang, Q.; Ke, S.; Qiu, L.; Zhang, X.; Lin, S. Palladium(II)/Polyoxometalate-Catalyzed Direct Alkenylation of Benzofurans under Atmospheric Dioxygen. *ChemCatChem* **2014**, *6*, 1531–1534.

(42) Pascanu, V.; Carson, F.; Solano, M. V.; Su, J.; Zou, X.; Johansson, M. J.; Martín-Matute, B. Selective Heterogeneous C-H Activation/Halogenation Reactions Catalyzed by Pd@MOF Nanocomposites. *Chem. - Eur. J.* **2016**, *22*, 3729–3737.

(43) Ferlin, F.; Santoro, S.; Ackermann, L.; Vaccaro, L. Heterogeneous C-H Alkenylations in Continuous-Flow: Oxidative Palladium-Catalysis in a Biomass-Derived Reaction Medium. *Green Chem.* **2017**, *19*, 2510–2514.

(44) Hu, Q.; Liu, X.; Wang, G.; Wang, F.; Li, Q.; Zhang, W. Ag1Pd1 Nanoparticles–Reduced Graphene Oxide as a Highly Efficient and Recyclable Catalyst for Direct Aryl C–H Olefination. *Chem. - Eur. J.* **2017**, *23*, 17659–17662.

(45) Cirujano, F. G.; Leo, P.; Vercammen, J.; Smolders, S.; Orcajo, G.; De Vos, D. E. MOFs Extend the Lifetime of Pd(II) Catalyst for Room Temperature Alkenylation of Enamine-Like Arenes. *Adv. Synth. Catal.* **2018**, *360*, 3872–3876.

(46) Liu, M.; Wu, J.; Hou, H. Metal–Organic Framework (MOF)-Based Materials as Heterogeneous Catalysts for C–H Bond Activation. *Chem. - Eur. J.* **2019**, *25*, 2935–2948.

(47) Otake, K.; Ye, J.; Mandal, M.; Islamoglu, T.; Buru, C. T.; Hupp, J. T.; Delferro, M.; Truhlar, D. G.; Cramer, C. J.; Farha, O. K. Enhanced Activity of Heterogeneous Pd(II) Catalysts on Acid-Functionalized Metal–Organic Frameworks. *ACS Catal.* **2019**, *9*, 5383–5390.

(48) Copéret, C.; Comas-Vives, A.; Conley, M. P.; Estes, D. P.; Fedorov, A.; Mougel, V.; Nagae, H.; Núnez-Zarur, F.; Zhizhko, P. A. Surface Organometallic and Coordination Chemistry toward Single-Site Heterogeneous Catalysts: Strategies, Methods, Structures, and Activities. *Chem. Rev.* **2016**, *116*, 323–421.

(49) Cui, X.; Li, W.; Ryabchuk, P.; Junge, K.; Beller, M. Bridging Homogeneous and Heterogeneous Catalysis by Heterogeneous Single-Metal-Site Catalysts. *Nat. Catal.* **2018**, *1*, 385–397.

(50) Corma, A.; García, H.; Llabrés i Xamena, F. X. Engineering Metal Organic Frameworks for Heterogeneous Catalysis. *Chem. Rev.* **2010**, *110*, 4606–4655.

(51) Gascon, J.; Corma, A.; Kapteijn, F.; Llabrés I Xamena, F. X. Metal Organic Framework Catalysis: Quo Vadis? *ACS Catal.* **2014**, *4*, 361–378.

(52) Rogge, S. M. J.; Bavykina, A.; Hajek, J.; Garcia, H.; Olivos-Suarez, A. I.; Sepúlveda-Escribano, A.; Vimont, A.; Clet, G.; Bazin, P.; Kapteijn, F.; Daturi, M.; Ramos-Fernandez, E. V.; Llabrés Xamena, F. X. I.; Van Speybroeck, V.; Gascon, J. Metal-Organic and Covalent Organic Frameworks as Single-Site Catalysts. *Chem. Soc. Rev.* **2017**, *46*, 3134–3184.

(53) Cirujano, F. G. Engineered MOFs and Enzymes for the Synthesis of Active Pharmaceutical Ingredients. *ChemCatChem* **2019**, *11*, 5671–5685.

(54) Dhakshinamoorthy, A.; Asiri, A. M.; Garcia, H. Formation of C-C and C-Heteroatom Bonds by C-H Activation by Metal Organic Frameworks as Catalysts or Supports. *ACS Catal.* **2019**, *9*, 1081–1102.

(55) Oien, S.; Agostini, G.; Svelle, S.; Borfecchia, E.; Lomachenko, K. A.; Mino, L.; Gallo, E.; Bordiga, S.; Olsbye, U.; Lillerud, K. P.; Lamberti, C. Probing Reactive Platinum Sites in UiO-67 Zirconium Metal–Organic Frameworks. *Chem. Mater.* **2015**, *27*, 1042–1056.

(56) Li, X.; Van Zeeland, R.; Maligal-Ganesh, R. V.; Pei, Y.; Power, G.; Stanley, L.; Huang, W. Impact of Linker Engineering on the Catalytic Activity of Metal-Organic Frameworks Containing Pd(II)-Bipyridine Complexes. *ACS Catal.* **2016**, *6*, 6324–6328.

(57) Chen, L.; Rangan, S.; Li, J.; Jiang, H.; Li, Y. A Molecular Pd(II) Complex Incorporated into a MOF as a Highly Active Single-Site Heterogeneous Catalyst for C-Cl Bond Activation. *Green Chem.* **2014**, *16*, 3978–3985.

(58) Leubner, S.; Zhao, H.; Van Velthoven, N.; Henrion, M.; Reinsch, H.; De Vos, D. E.; Kolb, U.; Stock, N. Expanding the Variety of Zirconium-based Inorganic Building Units for Metal–Organic Frameworks. *Angew. Chem., Int. Ed.* **2019**, *58*, 10995–11000.

(59) Anastasiou, I.; Van Velthoven, N.; Tomarelli, E.; Lombi, A.; Lanari, D.; Liu, P.; Bals, S.; De Vos, D. E.; Vaccaro, L. C2–H Arylation of Indoles Catalyzed by Palladium-Containing Metal-Organic-Framework in γ-Valerolactone. *ChemSusChem* **2020**, *13*, 1–7.

(60) Yang, D.; Odoh, S. O.; Borycz, J.; Wang, T. C.; Farha, O. K.; Hupp, J. T.; Cramer, C. J.; Gagliardi, L.; Gates, B. C. Tuning Zr6 Metal-Organic Framework (MOF) Nodes as Catalyst Supports: Site Densities and Electron-Donor Properties Influence Molecular Iridium Complexes as Ethylene Conversion Catalysts. *ACS Catal.* **2016**, *6*, 235–247.

(61) Li, Z.; Schweitzer, N. M.; League, A. B.; Bernales, V.; Peters, A. W.; Getsoian, A. B.; Wang, T. C.; Miller, J. T.; Vjunov, A.; Fulton, J. L.; Lercher, J. A.; Cramer, C. J.; Gagliardi, L.; Hupp, J. T.; Farha, O. K. Sintering-Resistant Single-Site Nickel Catalyst Supported by Metal-Organic Framework. *J. Am. Chem. Soc.* **2016**, *138*, 1977–1982.

(62) Manna, K.; Ji, P.; Lin, Z.; Greene, F. X.; Urban, A.; Thacker, N. C.; Lin, W. Chemoselective Single-Site Earth-Abundant Metal Catalysts at Metal-Organic Framework Nodes. *Nat. Commun.* **2016**, *7*, 1–11.

(63) Bernales, V.; Yang, D.; Yu, J.; Gümüşlu, G.; Cramer, C. J.; Gates, B. C.; Gagliardi, L. Molecular Rhodium Complexes Supported on the Metal-Oxide-like Nodes of Metal Organic Frameworks and on Zeolite HY: Catalysts for Ethylene Hydrogenation and Dimerization. *ACS Appl. Mater. Interfaces* **2017**, *9*, 33511–33520.

(64) Otake, K. I.; Cui, Y.; Buru, C. T.; Li, Z.; Hupp, J. T.; Farha, O. K. Single-Atom-Based Vanadium Oxide Catalysts Supported on Metal-Organic Frameworks: Selective Alcohol Oxidation and Structure-Activity Relationship. *J. Am. Chem. Soc.* **2018**, *140*, 8652–8656.

(65) Van Velthoven, N.; Waitschat, S.; Chavan, S. M.; Liu, P.; Smolders, S.; Vercammen, J.; Bueken, B.; Bals, S.; Lillerud, K. P.; Stock, N.; De Vos, D. E. Single-Site Metal–Organic Framework Catalysts for the Oxidative Coupling of Arenes via C–H/C–H Activation. *Chem. Sci.* **2019**, *10*, 3616–3622.

(66) Deria, P.; Bury, W.; Hod, I.; Kung, C. W.; Karagiaridi, O.; Hupp, J. T.; Farha, O. K. MOF Functionalization via Solvent-Assisted Ligand Incorporation: Phosphonates vs Carboxylates. *Inorg. Chem.* **2015**, *54*, 2185–2192.

(67) Fu, G.; Bueken, B.; De Vos, D. Zr-Metal-Organic Framework Catalysts for Oxidative Desulfurization and Their Improvement by Postsynthetic Ligand Exchange. *Small Methods* **2018**, *2*, 1800203.

(68) Zhang, W.; Bu, A.; Ji, Q.; Min, L.; Zhao, S.; Wang, Y.; Chen, J. PKa-Directed Incorporation of Phosphonates into MOF-808 via Ligand Exchange: Stability and Adsorption Properties for Uranium. *ACS Appl. Mater. Interfaces* **2019**, *11*, 33931–33940.

(69) Furukawa, H.; Gándara, F.; Zhang, Y.-B.; Jiang, J.; Queen, W. L.; Hudson, M. R.; Yaghi, O. M. Water Adsorption in Porous Metal-Organic Frameworks and Related Materials. *J. Am. Chem. Soc.* **2014**, *136*, 4369–4381.

(70) Thür, R.; Van Velthoven, N.; Lemmens, V.; Bastin, M.; Smolders, S.; De Vos, D.; Vankelecom, I. F. J. Modulator-Mediated Functionalization of MOF-808 as a Platform Tool to Create High-Performance Mixed-Matrix Membranes. *ACS Appl. Mater. Interfaces* **2019**, *11*, 44792–44801.

(71) Howarth, A. J.; Liu, Y.; Li, P.; Li, Z.; Wang, T. C.; Hupp, J. T.; Farha, O. K. Chemical, Thermal and Mechanical Stabilities of Metal-Organic Frameworks. *Nat. Rev. Mater.* **2016**, *1*, 1–15.

(72) Healey, K.; Liang, W.; Southon, P. D.; Church, T. L.; D'Alessandro, D. M. Photoresponsive Spiropyran-Functionalised MOF-808: Postsynthetic Incorporation and Light Dependent Gas Adsorption Properties. *J. Mater. Chem. A* **2016**, *4*, 10816–10819.

(73) Reinsch, H.; Waitschat, S.; Chavan, S. M.; Lillerud, K. P.; Stock, N. A Facile "Green" Route for Scalable Batch Production and Continuous Synthesis of Zirconium MOFs. *Eur. J. Inorg. Chem.* **2016**, *2016*, 4490–4498.

(74) Jia, C.; Cirujano, F. G.; Bueken, B.; Claes, B.; Jonckheere, D.; Van Geem, K. M.; De Vos, D. Geminal Coordinatively Unsaturated Sites on MOF-808 for the Selective Uptake of Phenolics from a Real Bio-Oil Mixture. *ChemSusChem* **2019**, *12*, 1256–1266.

(75) Bueken, B.; Van Velthoven, N.; Krajnc, A.; Smolders, S.; Taulelle, F.; Mellot-Draznieks, C.; Mali, G.; Bennett, T. D.; De Vos, D. Tackling the Defect Conundrum in UiO-66: A Mixed-Linker Approach to Engineering Missing Linker Defects. *Chem. Mater.* **2017**, *29*, 10478–10486.

(76) Thirunavukkarasu, V. S.; Donati, M.; Ackermann, L. Hydroxyl-Directed Ruthenium-Catalyzed C-H Bond Functionalization : Versatile Access to Fluorescent Pyrans. *Org. Lett.* **2012**, *14*, 14952–14955.

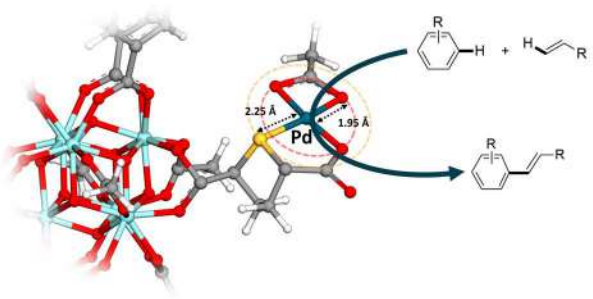
R
H
+
H
R
2.25 Å
1.95 Å
Pd
R
R